

Measurement of stiffness and damping constant of self-assembled monolayers

D. Devaprakasam and S. K. Biswas

Citation: [Review of Scientific Instruments](#) **76**, 035102 (2005); doi: 10.1063/1.1857278

View online: <http://dx.doi.org/10.1063/1.1857278>

View Table of Contents: <http://scitation.aip.org/content/aip/journal/rsi/76/3?ver=pdfcov>

Published by the [AIP Publishing](#)

Articles you may be interested in

[Contact resonance force microscopy with higher-eigenmode for nanoscale viscoelasticity measurements](#)

J. Appl. Phys. **116**, 034310 (2014); 10.1063/1.4890837

[Thermo-mechanical characterization of glass at high temperature using the cylinder compression test. Part II: No-slip experiments, viscoelastic constants, and sensitivity](#)

J. Rheol. **57**, 1391 (2013); 10.1122/1.4817435

[Modification of vibrational damping times in thin gold films by self-assembled molecular layers](#)

Appl. Phys. Lett. **98**, 261908 (2011); 10.1063/1.3604790

[Device for the independent verification of subresonant mechanical damping measurements](#)

Rev. Sci. Instrum. **74**, 2604 (2003); 10.1063/1.1561595

[Resonant ultrasound spectroscopy for measurement of mechanical damping: Comparison with broadband viscoelastic spectroscopy](#)

Rev. Sci. Instrum. **71**, 2855 (2000); 10.1063/1.1150703

Nor-Cal Products



Manufacturers of High Vacuum
Components Since 1962

- Chambers
- Motion Transfer
- Viewports
- Foreline Traps
- Valves

- Flanges & Fittings
- Feedthroughs



www.n-c.com
800-824-4166

Measurement of stiffness and damping constant of self-assembled monolayers

D. Devaprakasam^{a)} and S. K. Biswas^{b)}

Department of Mechanical Engineering, Indian Institute of Science, Bangalore 560 012, India

(Received 14 May 2004; accepted 20 December 2004; published online 15 February 2005)

We design and fabricate an apparatus which uses two dual double cantilever flexures to probe mechanical properties of self-assembled monolayers (SAM) under compression. The cantilevers were designed to give stiffness of the same order as the SAM. One of the cantilevers carrying the probe is vibrated sinusoidally at subresonance frequency and subnanometric amplitude while the dynamic response of the other carrying the SAM is recorded in the contact mode to yield data which could be deconvoluted to give stiffness and damping constant of the SAM under compression using a model of viscoelasticity. We validate the apparatus as well as the method of deconvolution by indenting bulk polytetrafluoroethylene and estimate mechanical properties of SAMs of different chain length and head group. The approach adopted here is able to distinguish in terms of mechanical properties a bulk polymer from a SAM and also between two SAMs of similar but subtly different structure. © 2005 American Institute of Physics. [DOI: 10.1063/1.1857278]

I. INTRODUCTION

The surface force apparatus designed and fabricated by Israelachvili and McGuiggan¹ was a breakthrough in measuring different types of surface forces valid at different length scales especially when molecules deposited on opposed surfaces interact in different media. While transparent substrate made up of materials such as mica is a must for implementation of high resolution displacement measurement using multiple beam interferometry, such an equipment has limited scope in engineering applications where surfaces are generally rough and substrate are opaque. The equipment designed and used by Corassous *et al.*² and Tonck *et al.*³ and later by Peachy *et al.*⁴ circumvents this problem and uses (AC) modulation, credited to Pethica and Oliver,⁵ to deconvolute elastic and damping properties of liquid molecules confined between engineering surfaces. The frequency dependent shear relaxation behavior of nonwetting molecules such as Octamethylcyclotetrasiloxane (OMCTS) is well documented.^{6,7} Joyce *et al.*⁸ have indicated that even in compression self-assembled monolayers (SAMs) possess time dependent elastic response. The problem we address here is the measurement of mechanical properties of a stiff polymeric monolayer assembled on a solid substrate. Such a problem is of interest to the designer of additive molecules used in tribology. The mechanical properties influence friction and load bearing capacity. Simple thiol molecules are known to have modulus of the order of 10 GPa.⁹ From the engineering point of view it is however the stiffness, a product of the storage modulus and the contact radius and the damping constant which have direct bearing on the load bearing capacity and friction.

The problem we address here imposes following restrictions on the configuration and design of an apparatus or selection of a standard equipment which may be used to measure the required properties. (1). The self-assembled monolayers are generally about 2–3 nm thick. To probe the properties of such a system the perturbation must be limited to about 20% of the thickness.¹⁰ At larger perturbation the molecular order is disturbed and the deconvoluted properties are composite properties of the test molecule and substrate.^{8,11} This rules out nanoindenter as a probing instrument, where the displacement resolution of this order is rarely achieved. (2). The contact area has to be large to allow the determination of average properties of a large number of molecules. This rules out the atomic force microscope (AFM) which has a tip of very small radius. (3). The relaxation time of SAMs of these test molecules are generally less than 0.1 s. The probe frequency has thus must be small, of the order of a few hertz. The stiffness of the measuring flexure cannot therefore also be too low as the low natural frequency leads to low signal-to-noise ratio. Further a low stiffness flexure is prone to snap-in instability which should be avoided. A very high stiffness of the flexure compared to that of the SAMs of molecules is also not acceptable as measurement of displacement of the order of 0.2–0.5 nm fall within the resolution of measurement system. We have in a previous paper¹² given the design of a dual double cantilever flexure system which is especially designed to nullify any rotation and sideways movement of a specimen platform of the type used in a surface force apparatus (SFA),⁷ on normal loading. Here two such cantilevers are part of an integral block, one is used to transmit a modulated displacement signal superposed on a ramp to a self-assembled monolayer deposited on a flat mounted on the second cantilever platform. The cantilevers are designed using the finite element method to satisfy the above requirements. This design gives a stiffness ($\approx 15\,000$ N/m) which is of the same order as the

^{a)}Research student.

^{b)}Professor; author to whom correspondence should be addressed; electronic mail: skbis@mecheng.iisc.ernet.in

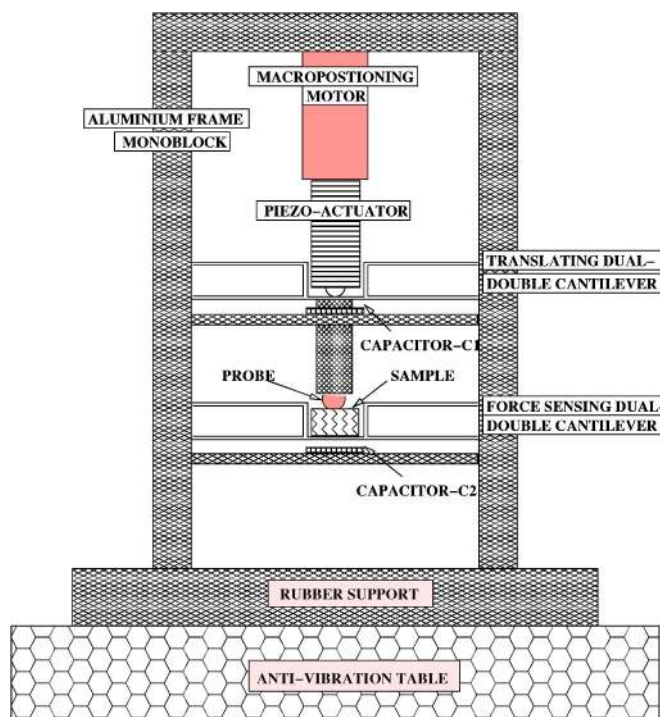


FIG. 1. Schematic of the apparatus (CFA) used for experimentation.

stiffness of the test samples. A similar approach has been used in the mechanical property measurement of confined water layers using an off-resonance AFM.¹³ High displacement resolution is achieved here by recording the sample displacement as a differential between the displacements of the two cantilevers, measured using capacitive sensors. We designate the equipment contact force apparatus.

Given the near solid state of the additive molecules we use the kelvin viscoelastic model^{14,15} to deconvolute the stiffness and damping properties of two stiff polymeric monolayers; perfluorooctyltrichlorosilane (FOTS) (Ref. 16) and perfluorooctadecylacid (PODA), self assembled on aluminum surfaces. As the stiffness of the self-assembled additive monolayers are not well known we first calibrate the instrument using a well-known polymer polytetrafluoroethylene (PTFE), the mechanical properties of which are well established.

II. EXPERIMENT

A schematic of the apparatus is shown in Fig. 1. It consists of two parallel and coaxial dual double cantilevers (DDC) integral to a main frame, the assembly is machined out of a single aluminum (Al—2024) block. A micromotor (Physik Instruments, Germany) is fixed at one end to the rigid frame while the other end is attached to a piezoactuator (Physik Instruments, Germany) which has a displacement resolution of 0.1 nm in a 10 μm range (electronic noise resolution 0.115 ppm/ $\sqrt{\text{Hz}}$). The actuator drives the top DDC platform, the underside of which is attached to the top end of a shank. The other end of the shank carries the indenter or the probe. The vertical displacement X of the top DDC platform is measured by a capacitor C1 of resolution 0.01 nm in a 15 μm range. The fixed plate of the capacitor is attached to

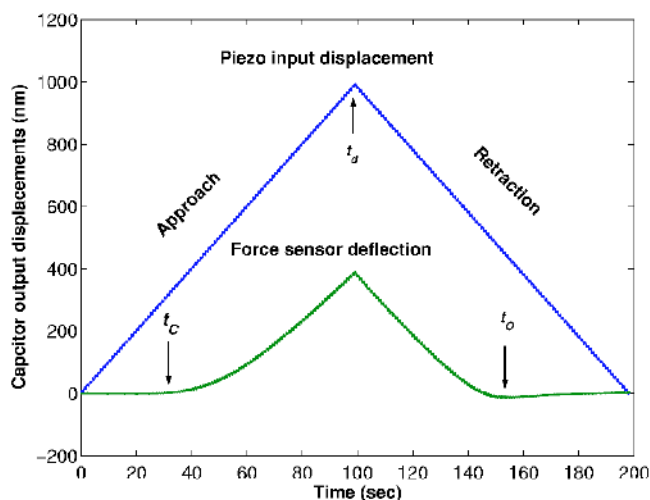


FIG. 2. Experimental result of piezodisplacement and bottom DDC deflection in nanometer plotted as function of time. t_c —contact begins, t_o —contact rupture, t_d —maximum displacement.

a plate fixed at both ends to the main frame. The indenter presses on the sample deposited on a substrate attached to the platform of the bottom DDC. The capacitor C2 (identical to C1) measures the deflection Y of the bottom DDC platform. The displacement of the probe tip with respect to the sample surface is given by $\delta = X - Y$. The force on the sample is given by $F = K_c Y$ where K_c is the cantilever stiffness (see Ref. 12 for calibration procedure). To measure the stiffness and damping of the sample a small AC signal (peak-peak: 1–10 nm, 1–100 Hz) is superposed on the actuator dc signal. Typical piezodisplacement (C1) and DDC displacement (C2) (force signal) are shown in Fig. 2.

Data is acquired using a 100 channel National Instruments (Austin, TX), data acquisition card (DAC) and visual C++ software. The rate of acquisition is 100 kS/s. The voltage signals from C1 and C2 are filtered and the signals fed into two dual phase lock-in amplifier (Stanford Research Systems, Sunnyvale, CA). The gain and phase are recorded. The piezoactuator is driven by a closed/open loop high voltage (0–1000 V) piezocontroller (Physik Instruments, Germany). The gain R and the phase φ are used to estimate the stiffness and damping constant of the sample.

A. Deconvolution of stiffness and damping constant

The spring-dashpot model of the system is shown in Fig. 3. where K_{pz} and K_{tr} are the stiffness of the piezoactuator and the top DDC spring and M_1 the effective mass of the probe and the top spring. K_c is the stiffness of the bottom DDC, i.e., force sensor and M_2 the effective mass of the sample substrate and the bottom DDC spring. K_s and C_s represent the stiffness and damping constant of the sample. Here we have ignored the damping effect of the capacitors which may be modeled as dashpots parallel to the top and bottom DDC springs. The capacitor plates are separated by a 10 μm air gap and we have measured the damping due to the air and found it to be negligible. Equation of motion for member 1 (M_1) is

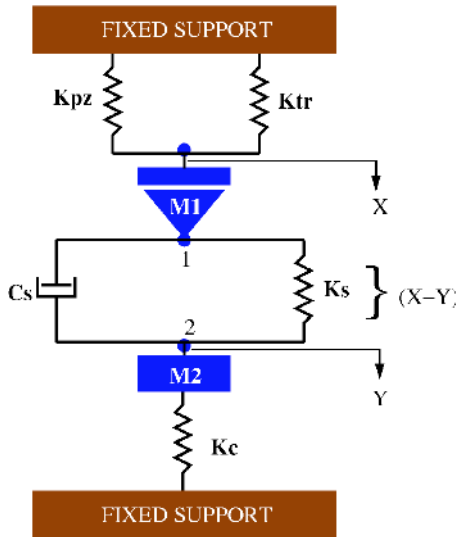


FIG. 3. Spring-dashpot model of CFA.

$$M_1 \ddot{X} + K_{\text{eff}} X = F_o e^{i\omega t}, \quad (1)$$

where K_{eff} is the effective stiffness of K_{pz} and K_{tr} . Since the operating frequency ($\omega \approx 1-100$ Hz) is less than the natural frequency ($\omega_o \approx 100$ KHz) of member 1, the inertia term $M_1 \ddot{X}$ can be neglected. As $K_{pz} \gg K_{tr}$ the effective stiffness $K_{\text{eff}} \approx K_{pz}$, Eq. (1) becomes

$$X = A_o e^{i\omega t},$$

where $A_o = (F_o / K_{pz})$ is the input amplitude. The combined equation of motion for member 2 (M_2) and the sample is

$$M_2 \ddot{Y} + K_c Y - C_s (\dot{X} - \dot{Y}) - K_s (X - Y) = 0. \quad (2)$$

Since the operating frequency (ω) is less than the natural frequency (ω_o) of member 2 the inertia term $M_2 \ddot{Y}$ can be neglected. Equation (2) becomes

$$K_c Y - C_s (\dot{X} - \dot{Y}) - K_s (X - Y) = 0. \quad (3)$$

The response equation of bottom DDC may be written as

$$Y = A_y \exp i(\omega t + \phi),$$

where A_y is the response amplitude. Substituting X and Y in Eq. (3), the real and imaginary parts of the equation may be separated. The real part is given by

$$(K_c + K_s) A_y \cos \phi - K_s A_o - \omega C_s A_y \sin \phi = 0$$

from which K_s is given as

$$K_s = \frac{K_c A_y \cos \phi - \omega C_s A_y \sin \phi}{(A_o - A_y \cos \phi)} = \frac{K_c R \cos \phi - \omega C_s R \sin \phi}{(1 - R \cos \phi)}, \quad (4)$$

where $R = A_y / A_o$. The imaginary part is

$$(K_c + K_s) A_y \sin \phi - \omega C_s A_o + \omega C_s A_y \cos \phi = 0$$

from which

$$\omega C_s = \frac{(K_c + K_s) A_y \sin \phi}{(A_o - A_y \cos \phi)} = \frac{(K_c + K_s) R \sin \phi}{(1 - R \cos \phi)}. \quad (5)$$

Solving Eqs. (4) and (5) gives the stiffness and damping constant of the sample material as

$$K_s = K_c \frac{(R \cos \phi - R^2)}{(R^2 - 2R \cos \phi + 1)}, \quad (6)$$

$$C_s = \frac{(K_c R \sin \phi)}{\omega (R^2 - 2R \cos \phi + 1)}. \quad (7)$$

It should be noted that the above model only analyzes the harmonic part of the experimental process. This serves the purpose of deconvolution of stiffness and damping constant of the sample. We have assumed that the elastic and viscous forces of the sample system are additive. This assumption is suitable for solid viscoelastic material, where stiffness and damping elements are parallel (Kelvin model).^{13,17,18} For liquids, Maxwell's visco-elastic model is more suitable where stiffness and damping elements act in series. The Kelvin model may be converted to Maxwell's using the following set of equations:

$$\eta_{\text{elastic}} = K_s + \frac{\omega^2 C_s^2}{K_s},$$

$$\eta_{\text{viscous}} = C_s + \frac{K_s}{\omega^2 C_s^2},$$

where η_{elastic} and η_{viscous} are the elastic and viscous components of the Maxwell model.

B. Storage (E') and loss (E'') moduli

Given K_s and ϕ we can now estimate the storage (E') and loss (E'') moduli. If ν_1, E_1 and ν_2, E_2 are the Poisson's ratio and Young's modulus of the probe and the sample material, respectively, and

$$\frac{1}{E_{\text{eff}}} = \frac{1 - \nu_1^2}{E_1} + \frac{1 - \nu_2^2}{E_2}.$$

We may estimate $E' = E_2$ from the above if we write using Sneddon's equation⁵

$$E_{\text{eff}} = \frac{K_s}{2a_c},$$

where a_c is the contact radius. For validation of the equipment and measurement procedure we measure the E' and E'' of a crystalline polymer, polytetrafluoroethylene (PTFE), the mechanical properties which are well established. For such a material we expect the material to flow at the asperity level on contact and result in the real area of contact to become about the same as the apparent area of contact. We thus assume a_c to be the Hertzian contact radius. We have measured the adhesion between the ruby sphere and the PTFE sample and found that the departure from the hertzian contact due to adhesion, is very small.²⁰ E'' is given by

$$E'' = E' \tan \phi.$$

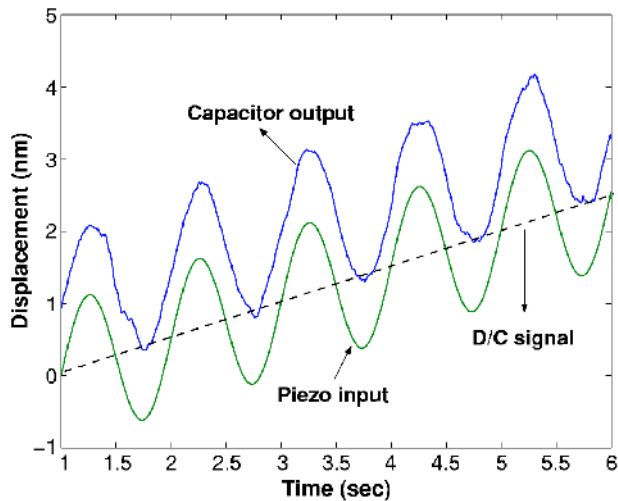


FIG. 4. Peak-to-peak calibration curve.

C. Calibration

Figure 4 shows an input (DC) ramp with a superposed 2 nm amplitude, 1 Hz, sinusoidal signal, and the corresponding capacitor response obtained in an experiment where the probe presses the bare Al substrate on bottom DDC. The gain is $R=1$ and the phase difference is $\phi=0$.

We next check the response of the system when a ruby tip of 1.12 mm radius indents an aluminum substrate. The aluminum substrate was polished to a rms (root mean square) roughness of 1 nm, ultrasonicated in 50–50 acetone water mixture, and dried in dry air. The experiment was conducted in a humidity chamber, at $\approx 10\%$ relative humidity. As the ruby sphere approaches the aluminum flat, the aluminum flat moves up to register a negative attractive force seen in Fig. 5. A contact is made at zero load. Figure 6 shows that the displacement of the ruby sphere in contact with the aluminum flat is the same as that of the aluminum flat in loading and unloading parts of the cycle as long as the interaction is in the contact mode. This gives rise to a vertical repulsive path without hysteresis, $\delta=X-Y=0$. This is seen in Fig. 5, which indicates that the aluminum flat is not indented. Figure 7 shows that the response (AC) amplitude (A_y) reaches the

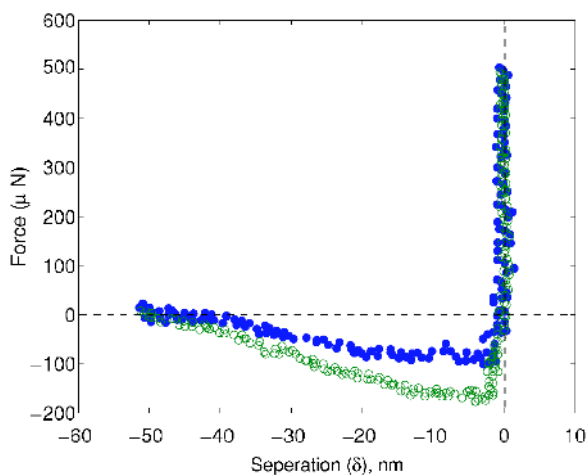
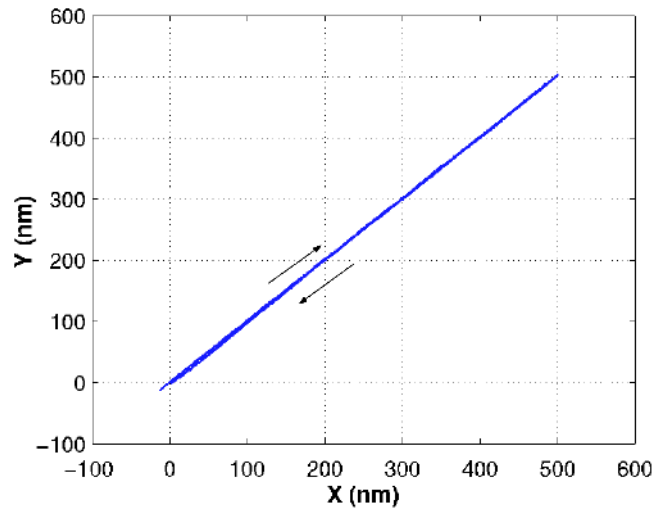


FIG. 5. Force curve of a ruby sphere (radius 1.12 mm) contacting an aluminum flat, loading (filled circle), unloading (open circle).

FIG. 6. Y (response) vs X (input), DC ramp, ruby sphere contacting an aluminum flat.

piezo (AC) amplitude ($A_o=2$ nm) and the phase difference becomes zero as soon as the tip makes contact with the substrate, t_{loc} in Fig. 7 is the characteristic time of the lock-in amplifier to lock the signal, t_{loc} is related to the proportional integral differential (PID) value selected for the amplifier. The phase angle remains zero at all loads during the experiment.

D. Validation of the spring-dashpot model

We validate the model by penetrating a polymer, polytetrafluoroethylene (PTFE) of low modulus and deconvolute the storage and loss modulus from the machine data of gain and phase difference.

A disc of thickness 1 cm was cut out from PTFE rod of 1 cm diameter (Reliance Plastics, India; the manufacturer specifies a Young's modulus of ≈ 0.4 GPa) and polished using commercially available polishing cloth. The experiments were performed using a ruby sphere of radius 1.12 mm. An AC signal of 5 nm amplitude and 5 Hz frequency was superposed on the DC ramp.

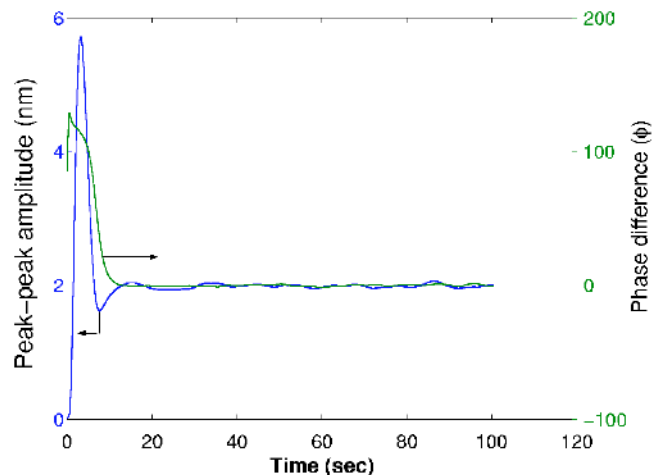


FIG. 7. Response of capacitor C2 to a piezo-(AC) signal of 2 nm peak-to-peak amplitude. Ruby sphere (1.12 mm radius) approaching an aluminum flat.

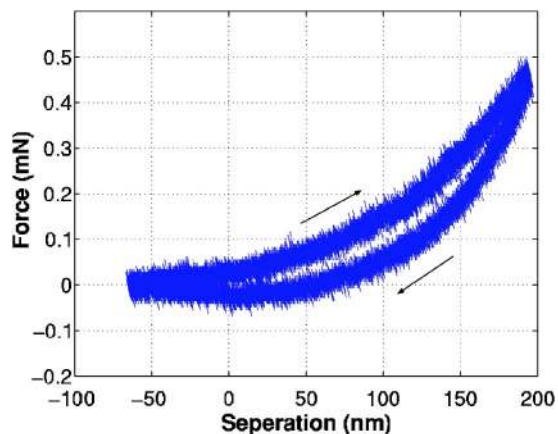


FIG. 8. Load-displacement curve from indentation of PTFE disc.

Figure 8 shows a load-displacement curve with a hysteresis. Figure 9 shows the stiffness and damping constant of PTFE as a function of penetration. It is of interest to note that the damping constant increases with penetration of this relatively thick PTFE film. Figure 10 shows the deconvoluted storage and loss modulus. The estimated values of these moduli agree with those given in the literature.¹⁹

III. MECHANICAL PROPERTIES OF SELF ASSEMBLED MONOLAYER

The thickness of a self-assembled monolayer is generally of the order of 2–3 nm. We propose to deconvolute the stiffness and damping coefficient of a SAM in the contact mode. The aluminum substrate was prepared as stated before. 1 mM FOTS in isooctane was prepared and the aluminum substrate was dipped in it for 30 min. The substrate was taken out, washed in isooctane, and again dried in dry nitrogen gas and preserved in a vacuum desiccator prior to experiments. Grazing angle Fourier transform infrared (Perkin-Elmer, Germany) was used to obtain spectra of the deposited film to ensure monomolecular coverage of the substrate by the SAM. The same procedure as used for the preparation of FOTS SAM was done for the preparation of perfluorooctadecylacid (PODA), except that the solvent used was chloro-

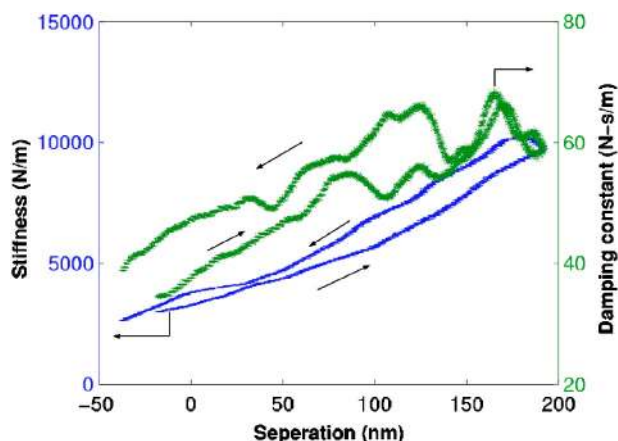


FIG. 9. Stiffness and damping constant of PTFE as a function of separation, positive value of separation is penetration. The arrows to the right and left are the loading and unloading, respectively.

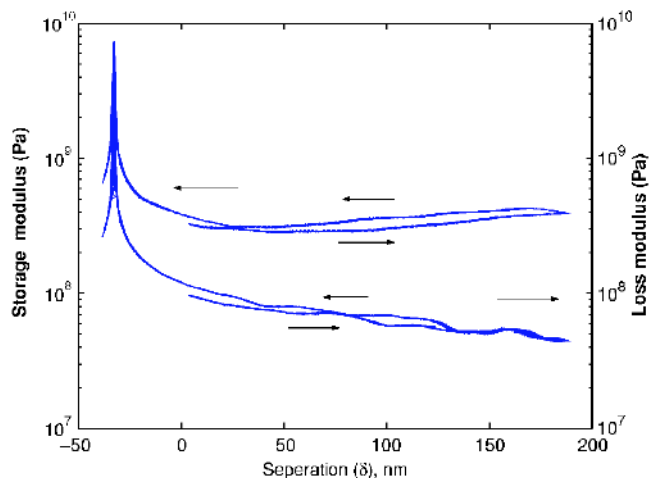


FIG. 10. Storage and loss moduli of PTFE as a function of separation. The arrows to the right and left are the loading and unloading, respectively.

form and the substrate was dipped in the solution for four hours. A ruby sphere of 1.12 mm radius was used to contact the SAM. The experiments were conducted using an AC signal of 1 nm peak to peak amplitude and 5 Hz frequency. Figure 11 shows the force-displacement characteristics of FOTS obtained in a DC mode ($A_o=0$ nm). It is clear that there is an approach to the sample over a ≈ 10 nm distance where the force is attractive. Very close to zero separation the force increases sharply with minimal displacement. If we mark this point of inflexion as contact the displacement does not change measurably beyond this value even when the load increases to 100 μ N, on retraction no appreciable hysteresis is observed. It should be noted that the experiment using present apparatus gives the attractive part of the force in the noncontact approach and retraction regimes. It should be reiterated at this stage that no indentation of the aluminum substrate was observed (Fig. 5) even at 500 μ N load. The maximum load used in probing FOTS SAM (120 μ N) is thus unlikely to result in any indentation of the substrate. Figure 12 shows the stiffness characteristics for FOTS de-

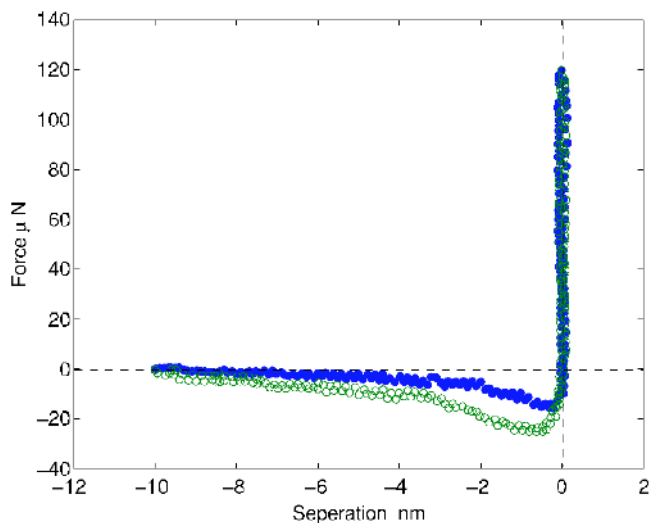


FIG. 11. Force curve of a ruby sphere (radius 1.12 mm) contacting FOTS on aluminum flat, loading (filled circle), unloading (open circle).

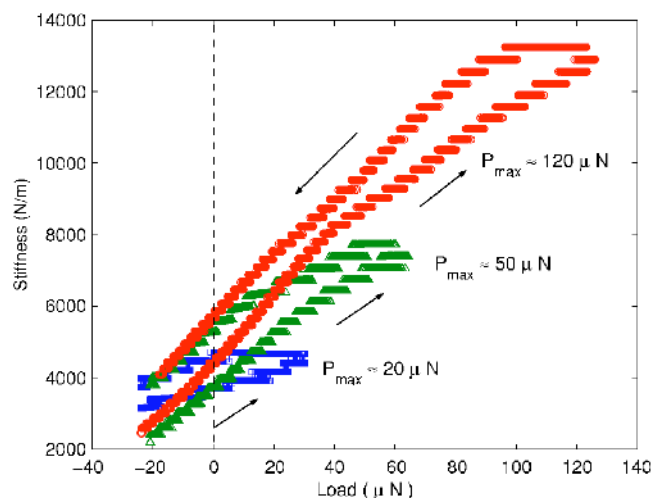


FIG. 12. Stiffness of FOTS as a function of applied load. Note the positive stiffness in the noncontact regime. P_{\max} is maximum load applied. The arrows to the right and left are the loading and unloading, respectively.

convoluted using Eq. (6) for different peak loads. Figure 12 gives some idea of the experimental variation from three independent experiments. It also shows that the stiffness starts to increase long before contact (zero load). The maximum attractive force recorded here is about $20 \mu\text{N}$ which is significantly less than that ($\approx 920 \mu\text{N}$) due to any possible capillary effect.¹ Considering that the experiments were done at about 10% RH (relative humidity), this perhaps is not surprising. We are thus led to believe that the recorded non-contact attraction is most probably due to the presence of van der Waal forces. The damping constant obtained using Eq. (7) also increases (Fig. 13) in the noncontact regime and attains a peak at about $+30 \mu\text{N}$ for the FOTS SAM. It should be noted at this stage that the driving frequency which is low in these experiments allows significant time for the molecule to relax. Compared to the 0.08 s relaxation time constants estimated for thiol SAM (Ref. 8) the driving time constant here is 0.2 s. At the higher loads the damping constant for both the test SAMs decrease and attains zero value at 80 and $120 \mu\text{N}$ for PODA and FOTS SAMs, respectively. Both the

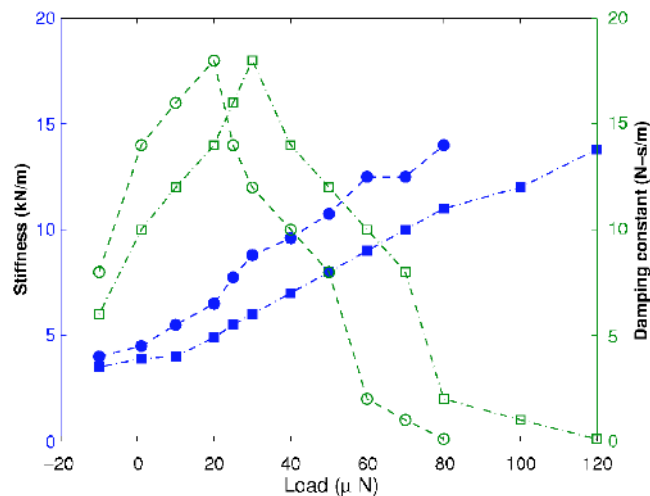


FIG. 13. Stiffness (filled symbols) and damping constant (open symbols) of FOTS (square) and PODA (circle) as a function of load.

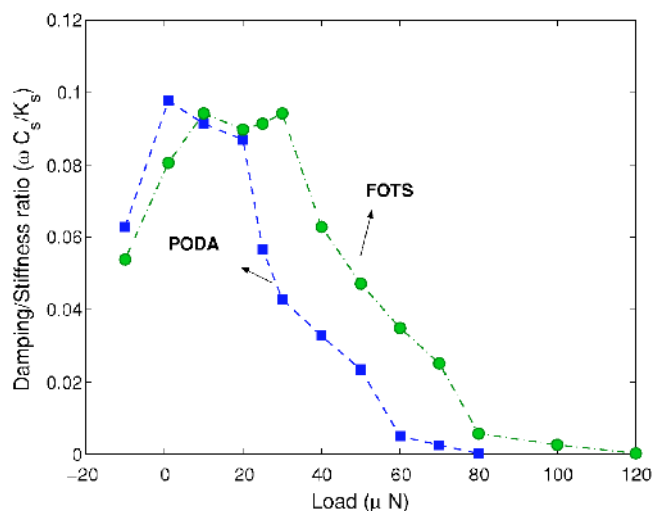


FIG. 14. $\omega C_s/K_s$ ratio of FOTS (circle) and PODA (square) as a function of load. Note the transition from viscous to elastic response.

test molecules broadly show the same characteristics, the stiffer PODA molecule with acid head group relaxes faster than the FOTS molecule with silane head group and attains zero damping at lower compressive loads. If a nondimensional damping-constant-to-stiffness ratio represents a notional ratio of liquidlike-to-solidlike behavior we see in Fig. 14 a sharp transition for the two SAMs at a rate of $1600/\text{N}$ in the $20\text{--}100 \times 10^{-6} \text{ N}$ range. For PTFE the ratio (extracted from Fig. 9) is 0.4 at zero load and it decreases almost asymptotically to 0.2 over a load range of $0\text{--}2.5 \times 10^{-3} \text{ N}$ at an average rate of about $80/\text{N}$. Thus the bulk PTFE unlike the SAMs shows a model viscoelastic behavior, never quite becoming nondissipative even at high loads. The SAMs on the other hand show a sharp transition from viscous to purely elastic response behavior at a compression load which is specific to the structure of the molecules being tested.

ACKNOWLEDGMENTS

The authors are grateful to DRDO (India) and General Motors (R and D) Warren, MI for grants used to support this work.

- ¹J. N. Israelachvili and P. M. McGuiggan, *J. Mater. Res.* **5**, 2223 (1990).
- ²J. Crassous, E. Charlaix, and J. L. Loubet, *Phys. Rev. Lett.* **78**, 2425 (1997).
- ³A. Tonck, J. M. Georges, and J. L. Loubet, *J. Colloid Interface Sci.* **126**, 150 (1993).
- ⁴J. Peachey, J. Van Alsten, and S. Granick, *Rev. Sci. Instrum.* **62**, 463 (1991).
- ⁵J. B. Pethica and W. C. Oliver, *Phys. Scr.*, T **T19**, 61 (1987).
- ⁶A. L. Demirel and S. Granick, *Phys. Rev. Lett.* **77**, 2261 (1996).
- ⁷A. L. Demirel and S. Granick, *J. Phys.: Condens. Matter* **8**, 9537 (1996).
- ⁸S. A. Joyce, R. C. Thomas, J. E. Houston, T. A. Michalske, and R. M. Crooks, *Phys. Rev. Lett.* **68**, 2790 (1992).
- ⁹A. R. Burns, J. E. Houston, R. W. Carpick, and T. A. Michalske, *Langmuir* **15**, 2922 (1999).
- ¹⁰I. Siepmann and I. R. McDonald, *Phys. Rev. Lett.* **70**, 453 (1993).
- ¹¹R. A. Quon, A. Ulman, and T. K. Vanderlick, *Langmuir* **16**, 3797 (2000).
- ¹²D. Devaprakasam and S. K. Biswas, *Rev. Sci. Instrum.* **74**, 1228 (2003).
- ¹³S. Jeffery, P. M. Hoffmann, J. B. Pethica, C. Ramanujan, H. O. Ozer, and A. Oral, cond-mat/03120219 v1 9 Oct 2003.
- ¹⁴W. N. Findley, J. S. Lai, and K. Onaran, *Creep and Relaxation of Nonlinear Viscoelastic Materials* (Dover, New York, 1976).

- ¹⁵J. D. Ferry, *Viscoelastic Properties of Polymers* (Wiley, New York, 1980).
- ¹⁶D. Devaprakasam, S. Sampath, and S. K. Biswas, *Langmuir* **20**, 1329 (2004).
- ¹⁷G. Luengo, F.-J. Schmitt, R. Hill, and J. N. Israelachvili, *Macromolecules* **30**, 2482 (1997).
- ¹⁸R. A. Oral, H. Grimple, O. Ozer, and J. B. Pethica, *Rev. Sci. Instrum.* **74**, 3656 (2003).
- ¹⁹B. N. Lucas, C. T. Rosenmeyer, and W. C. Oliver, *Mechanical Characterisation of Sub-micron Polytetrafluoroethylene Thin Films*, MRS fall meeting, Boston, MA (Essex South (W)), Los Alamos National Laboratory, 1997).
- ²⁰K. L. Johnson, *Contact Mechanics*, (Cambridge University Press, UK, 1985).